Image reconstruction based on total-variation minimization and alternating direction method in linear scan computed tomography*

Zhang Han-Ming(张瀚铭), Wang Lin-Yuan(王林元), Yan Bin(闫 镔)†,
Li Lei(李 磊), Xi Xiao-Qi(席晓琦), and Lu Li-Zhong(陆利忠)

National Digital Switching System Engineering and Technological Research Center, Zhengzhou 450002, *China*

(Received 6 September 2012; revised manuscript received 17 December 2012)

Linear scan computed tomography (LCT) is of great benefit to online industrial scanning and security inspection due to its characteristics of straight-line source trajectory and high scanning speed. However, in practical applications of LCT, there are challenges to image reconstruction due to limited-angle and insufficient data. In this paper, a new reconstruction algorithm based on total-variation (TV) minimization is developed to reconstruct images from limited-angle and insufficient data in LCT. The main idea of our approach is to reformulate a TV problem as a linear equality constrained problem where the objective function is separable, and then minimize its augmented Lagrangian function by using alternating direction method (ADM) to solve subproblems. The proposed method is robust and efficient in the task of reconstruction by showing the convergence of ADM. The numerical simulations and real data reconstructions show that the proposed reconstruction method brings reasonable performance and outperforms some previous ones when applied to an LCT imaging problem.

Keywords: linear scan CT, image reconstruction, total variation, alternating direction method

PACS: 87.59.–e, 07.85.–m, 87.57.Q– **DOI:** 10.1088/1674-1056/22/7/078701

1. Introduction

Computed tomography (CT) has become a widely-used imaging technology in various applications of industrial nondestructive testing (NDT) and medical fields for its advantages of fast speed, high precision, high spatial resolution, etc. Traditionally, imaging trajectories for CT are either circular or helical. As the technology evolves, more and more trajectories have been investigated for specific applications.[1–3] Linear scan computed tomography (LCT) is useful in fields like industrial scanning and security inspection due to its geometric and physical features.[4,5] The LCT scanning configuration could be executed physically in many ways. Here, we only focus on the way in which the X-ray source and the detector would remain stationary, and the object to be scanned is moved on a straight line. Compared with circular or helical scanning mode, LCT mode needs no rotation, its mechanical design and control are relatively easy to implement. Hence, the scanning speed could be rapid and it is terrific for the applications of online industrial testing and security inspection. Meanwhile, it is also applied to the NDT for the objects that are long and straight. Consequently, the LCT has become one of the research hotspots in the fields of CT and the research of the LCT image reconstruction has aroused the substantial interest.

The analytical method has been adopted widely in practical reconstruction due to its less computational complexity and acceptable result in the CT image reconstruction field. For the straight-line trajectory, the convolution backprojection algorithm,[6] the direct filtered backprojection type algorithm,[7] the backprojection filtration (BPF) algorithm,[8] and many other analytical approaches[9] were studied. However, these algorithms obtain the exact reconstruction only on condition that the source trajectory line segment goes to infinite length where the Tuy's sufficiency condition[10] is satisfied. In practical applications, the LCT's effective coverage of projection angle φ is less than π, so it is a limited-angle problem. To solve this problem, Gao *et al.*[7] introduced an iterative reconstruction reprojection (IRR) method to reduce the artifacts, and then, they presented an iterative Gerchberg–Papoulis-type extrapolation (GPEL) method for the compensation for missing data in LCT image reconstruction in Fourier domain.[11]

The compressive sensing (CS) theory by Candes *et al.*[12,13] provided a method of exactly recovering an image from the sparse samples of its discrete Fourier transform (DFT). The exact recovery depends on the fact that there exists some representations of the image for which the corresponding coefficients are sparse. Sparsity of images is generally not widely applicable in industrial or security scanning applications, but it is often the case that the images have sparse gradient-magnitude images (GMI).[14] For such images, minimizing the image total variation (TV), which is the l_1-norm of the GMI and subject to the data constraint, can yield the accurate images from sparse DFT samples. Recently, the method based on the corresponding constrained TV or l_1-norm minimization was widely studied in the reconstruction from few-view and limited-angle data.[14–22]

*Project supported by the National High Technology Research and Development Program of China (Grant No. 2012AA011603).

†Corresponding author. E-mail: ybspace@yahoo.com.cn

Gao *et al.*[15] combined TV regularization with the GPEL iteration and obtained a GPEL-TV method to restrain the noise and oscillation. Chen *et al.*[16] used a prior image reconstructed from the union of interleaved dynamical data sets to constrain the CS image reconstruction[16] Sidky *et al.*,[17] and Sidky and Pan[14] proposed the adaptive steepest descent-projection onto convex sets (ASD-POCS) algorithm in CT image reconstruction. The ASD-POCS algorithm was a combination of gradient descent on the TV-objective function and POCS to enforce the data and positivity constraints. And in the past few years it has been shown that the algorithms based on ASD-POCS framework were able to handle incomplete datasets quite well and realize excellent performance in sparse-view CT applications.[18–21] But it is pointed out that the ASD-POCS algorithm has a problem of how to find a system to balance TV-gradient descent with POCS, and the balance was achieved by making the TV-gradient-descent step-size proportional to the change in the image due to the POCS.[14]

In this paper, we intend to make some further contributions to the subject in reconstructing an image from limited-angle based on TV minimization method, and improve the performance by the use of alternating direction method (ADM) which minimizes the augmented Lagrangian functions through an alternating minimization scheme. We demonstrate the correctness and virtues of the proposed method by numerical examples through using projection data in a limited angular range. In the numerical examples, we find that the reconstruction quality and efficiency of the proposed method are improved compared with the ASD-POCS method.

The rest of this paper is organized as follows. In Section 2, we formulate a TV minimization algorithm based on ADM for LCT image reconstruction. Experimental results as well as the comparisons with those obtained by the widely used ASD-POCS algorithm are presented in Section 3. Finally, conclusions and discussion are given in Section 4.

2. Method

2.1. LCT systematic description

The configuration of LCT in this paper is the same as the one in Ref. [7]. It is schematically illustrated in Fig. 1(a). Both the X-ray source and the detector would remain stationary and the object scanned is moved on a straight line. This is equivalent to fixing the object and having the source and the detector translated by the object.

Figure 1(b) shows the geometry of the LCT scanning. Let O denote the origin in the object coordinates (x,y). An equivalent detector horizontally passing the origin O is used. The source is indexed by l which is its offset from O', each detector element is indexed by t which is its offset from O''. The distance from the source to the equivalent detector is D. Hence, the projection $p(l,t)$ is the line integral along the ray AB passing though the source trajectory at l and the detector element at t.

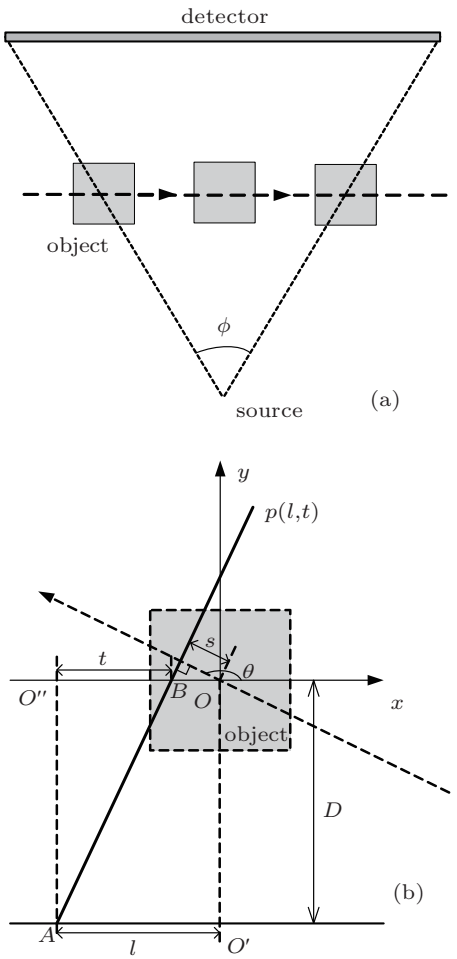

Fig. 1. Systematic description of LCT, showing (a) the scan geometry and (b) projection data geometry.

As shown in Fig. 1(b), one projection datum $p(l,t)$ will correspond to one angle, the datum from each detector element corresponds to a certain view angle of parallel beams. Thus, $p(l,t)$ from an object function $f(x,y)$ can be written as

$$\begin{aligned} p(l,t) &= \iint f(x,y)\delta(x\cos\theta + y\sin\theta - s)\,\mathrm{d}x\mathrm{d}y \\ &= \iint f(x,y)\frac{\sqrt{D^2+t^2}}{D}\delta(x - y\frac{t}{D} - l - t)\,\mathrm{d}x\mathrm{d}y, \quad (1) \end{aligned}$$

with $\theta = \pi - \tan^{-1}(t/D)$ and $s = -D(l+t)/\sqrt{D^2+t^2}$ being the corresponding view angle and detector position in the parallel-beam scan geometry, respectively.

2.2. TV minimization reconstruction based on ADM for LCT

The imaging model, equation (1), can be approximated by the following discrete linear system:

$$p = W\boldsymbol{f}. \quad (2)$$

The vector p represents the data obtained from measured projection rays; the vector $\boldsymbol{f}$ has the length which is equal to

the number of expansion elements used for representing the object function $f(x,y)$; and the system matrix W is a discrete model for the integration in Eq. (1).

In LCT systems, the projection data are not sufficient for exact reconstruction. Mathematically, the problem considered here involves insufficient data, and the reconstruction is ill-posed. To solve the linear system represented in Eq. (2), we specify a TV algorithm that implements the following optimization program. Constrained TV minimization yields the discrete image $\boldsymbol{f}$ that minimizes its TV as follows:

$$\begin{aligned} &\boldsymbol{f}^* = \arg\min \|\boldsymbol{f}\|_{\mathrm{TV}}, \\ &\text{subject to (s.t.)} \quad p = W\boldsymbol{f}, \boldsymbol{f} \geq 0. \end{aligned} \tag{3}$$

Let u_i equal the discrete gradient of $\boldsymbol{f}$ at pixel i, then we will obtain the TV model as follows:

$$\min \sum_i \|u_i\|, \quad \text{s.t.} p = W\boldsymbol{f} \text{ and } D_i\boldsymbol{f} = u_i. \tag{4}$$

For the constrained optimization, an influential class of method seeks for the minimizer or maximizer by the original constrained problem approached by a sequence of unconstrained subproblems. A well-known one is the augmented Lagrangian method, which could be regarded as a combination of the Lagrangian and quadratic penalty functions.

The corresponding augmented Lagrangian function of formula (4) is

$$\begin{aligned} L_{\mathrm{A}}(\boldsymbol{f}, u_i) = &\sum_i \left(\|u_i\| - \nu_i^{\mathrm{T}}(D_i\boldsymbol{f} - u_i) + \frac{\beta_i}{2} \cdot \|D_i\boldsymbol{f} - u_i\|_2^2 \right) \\ &- \lambda^{\mathrm{T}}(W\boldsymbol{f} - p) + \frac{\mu}{2} \cdot \|W\boldsymbol{f} - p\|_2^2. \end{aligned} \tag{5}$$

Let $(\boldsymbol{f}^*, u_i^*)$ represent the true minimizer of Eq. (5), the update formulas of multipliers follow

$$\widetilde{\nu}_i = \nu_i - \beta_i(D_i\boldsymbol{f}^* - u_i^*) \quad \widetilde{\lambda} = \lambda - \mu(W\boldsymbol{f}^* - p). \tag{6}$$

The task of solving problem (4) is equal to minimizing $L_{\mathrm{A}}(\boldsymbol{f}, u_i)$ efficiently at each iteration. The alternating direction method[23–25] is used here to solve the minimization of Eq. (5) efficiently.

Suppose that $(\boldsymbol{f}^k, u_i^k)$ denotes the approximate minimizer of Eq. (5) at the k-th iteration which refers to the inner iteration while solving the subproblem. Assuming that u_i^{k+1} can be attained by

$$\begin{aligned} &\min_{u_i} L_{\mathrm{A}}\left(\boldsymbol{f}^k, u_i\right) \\ &= \sum_i \left(\|u_i\| - \nu_i^{\mathrm{T}}\left(D_i\boldsymbol{f}^k - u_i\right) + \frac{\beta_i}{2} \cdot \left\|D_i\boldsymbol{f}^k - u_i\right\|_2^2 \right) \\ &\quad - \lambda^{\mathrm{T}}\left(W\boldsymbol{f}^k - p\right) + \frac{\mu}{2} \cdot \left\|W\boldsymbol{f}^k - p\right\|_2^2, \end{aligned} \tag{7}$$

which is equivalent to solving the so-called "u-subproblem"

$$\min_{u_i} \sum_i \left(\|u_i\| - \nu_i^{\mathrm{T}}\left(D_i\boldsymbol{f}^k - u_i\right) + \frac{\beta_i}{2} \cdot \left\|D_i\boldsymbol{f}^k - u_i\right\|_2^2 \right). \tag{8}$$

With the aid of u_i^{k+1}, $\boldsymbol{f}^{k+1}$ can be achieved by solving

$$\begin{aligned} &\min_{\boldsymbol{f}} L_{\mathrm{A}}\left(\boldsymbol{f}, u_i^{k+1}\right) \\ &= \sum_i \left(\left\|u_i^{k+1}\right\| - \nu_i^{\mathrm{T}}\left(D_i\boldsymbol{f} - u_i^{k+1}\right) + \frac{\beta_i}{2} \cdot \left\|D_i\boldsymbol{f} - u_i^{k+1}\right\|_2^2 \right) \\ &\quad - \lambda^{\mathrm{T}}(W\boldsymbol{f} - p) + \frac{\mu}{2} \cdot \|W\boldsymbol{f} - p\|_2^2, \end{aligned} \tag{9}$$

which is equivalent to solving the so-called "f-subproblem"

$$\begin{aligned} &\min_{\boldsymbol{f}} D_k(\boldsymbol{f}) \\ &\triangleq \sum_i \left(-\nu_i^{\mathrm{T}}\left(D_i\boldsymbol{f} - u_i^{k+1}\right) + \frac{\beta_i}{2} \cdot \left\|D_i\boldsymbol{f} - u_i^{k+1}\right\|_2^2 \right) \\ &\quad - \lambda^{\mathrm{T}}(W\boldsymbol{f} - p) + \frac{\mu}{2} \cdot \|W\boldsymbol{f} - p\|_2^2. \end{aligned} \tag{10}$$

$D_k(\boldsymbol{f})$ is a quadratic function, and its gradient is

$$\begin{aligned} d_k(\boldsymbol{f}) = &\sum_i \left(\beta_i D_i^{\mathrm{T}}\left(D_i\boldsymbol{f} - u_i^{k+1}\right) - D_i^{\mathrm{T}}\nu_i \right) \\ &+ \mu W^{\mathrm{T}}(W\boldsymbol{f} - p) - W^{\mathrm{T}}\lambda. \end{aligned} \tag{11}$$

Setting $d_k(\boldsymbol{f}) = 0$ gives us the exact minimizer of $D_k(\boldsymbol{f})$ as follows:

$$\begin{aligned} \boldsymbol{f}^{k+1^*} = &\left(\sum_i \beta_i D_i^{\mathrm{T}} D_i + \mu W^{\mathrm{T}} W \right)^{+} \left(\sum_i \left(D_i^{\mathrm{T}}\nu_i + \beta_i D_i^{\mathrm{T}} u_i^{k+1} \right) \right. \\ &\left. + W^{\mathrm{T}}\lambda + \mu W^{\mathrm{T}} p \right). \end{aligned} \tag{12}$$

Here, M^+ denotes the Moore–Penrose pseudo inverse of matrix M. The augmented Lagrangian function (5) is expected to be minimized by solving u-subproblem (8) and f-subproblem (10) alternately.

It is noticeable that this iteration is a kind of TV regularization algorithm which is based on the idea of alternating direction minimization to solve subproblems. Thus, the above iterative is called alternating direction total variation minimization (ADTVM) method in this paper.

3. Experimental results

To demonstrate and validate the presented ADTVM method of the image reconstruction, we implemente it and evaluate it with both numerical simulation data and real CT data. All experiments are performed in the C programming language under Visual Studio 2005 running on a Lenovo ThinkStation D20 with Intel Xeon E5620 CPU 2.40 GHz (only one processor was used) and 24 GB of memory. And it is noted that we partly refer to the Rice Matlab solver of "TVAL3"[23] in the implementation.

3.1. Simulation studies

To bring forth the advantages of the presented ADTVM method, we perform the following numerical experiments. Two kinds of configurations are simulated: one segment for an angle range of 90° and two segments for each angle range of 45°. The benefits from the second configuration are that not only each angle of X-ray beam coverage can be small but also the total length of the detector array can be short.

The scanning and reconstruction parameters are listed in Table 1, and detector elements are equidistantly spaced with 10 mm. The sampling step in source translation is 2 mm. The perpendicular distances from the source to the object center and to the detector are 512 nm and 1280 mm in the configuration 1 (618.4 mm and 1546 mm in configuration 2), respectively. Hence, the equivalent sample interval on the equivalent detector is 4 mm.

Table 1. Parameters in an LCT scan.

Parameters	Configuration 1	Configuration 2
Number of segments	1	2
Detector elements in one segment	256	256
Detector length in one segment	2560 mm	1280 mm
Source to axis distance	512 mm	618.4 mm
Source to detector distance	1280 mm	1546 mm
Source to equivalent detector distance	512 mm	618.4 mm
Equivalent detector length in one segment	1024 mm	512 mm
Views of projection data	128	64×2
Projection data	256×128	256×64×2
Reconstruction size	256×256 pixels	256×256 pixels
Pixel size	2^2 mm^2	2^2 mm^2

To validate how the ADTVM method can be applied to LCT scanning, we make a comparison with the ASD-POCS algorithm. Different choices of parameters of ASD-POCS algorithm have been tried, and at the end we pick out the ones that provide the best performance measured by recovery quality and running time.

In the first configuration, we use one detector for data acquisition by taking 128 angular samples distributed over an angle range of only 90°. For this scan, the sampling data in the Fourier space is in a two-opposite-triangular region (shown in Fig. 2). For this study, the projection data are generated for the Shepp–Logan phantom at 128 views in a coverage of 90°. The size of the phantom simulation is set as follows: the image size is $256 \times 256 = 65536$ voxels, and the projection data size is 128 views with 256 detectors or 32768 measured rays.

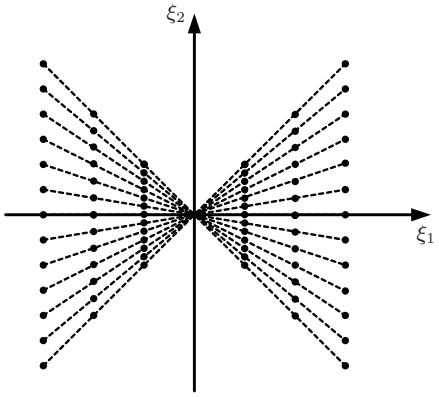

Fig. 2. Sampling points of a 90° scan in the Fourier space.

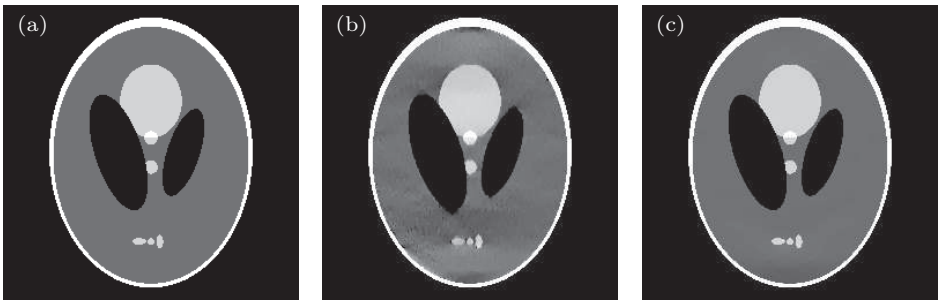

Fig. 3. Image reconstructions of the Shepp–Logan phantom in 90° LCT scan. Display window [0.1, 0.35]. Panel (a) shows the original image, panel (b) the result of ASD-POCS algorithm, and panel (c) the result of ADTVM algorithm.

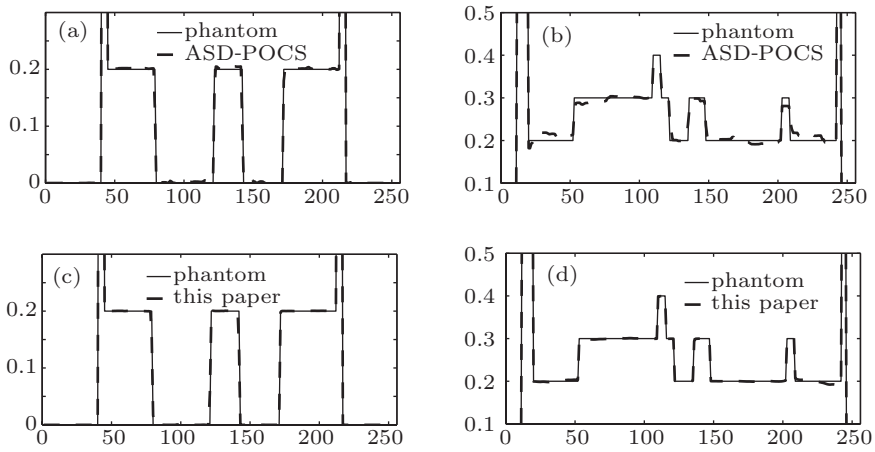

Fig. 4. Image profiles in Fig. 3, showing (a) horizontal profiles along the center of the ASD-POCS result, (b) vertical profiles along the center of the ASD-POCS result, (c) horizontal profiles along the center of the ADTVM result, and (d) vertical profiles along the center of the ADTVM result.

The images reconstructed from this set of data by using the ADTVM and ASD-POCS algorithms are shown in Fig. 3. The profiles of these images along the central horizontal and vertical rows are displayed in Fig. 4. The numbers of iterations for ADTVM and ASD-POCS reconstructions are both 1000.

The profiles in Fig. 4 show that the ADTVM reconstruction contains a little deviation from the true phantom near the bottom of the image and the ASD-POCS reconstruction has some distortions, which is evident in the shown profile plots.

To demonstrate the reconstruction accuracy quantitatively, we use the root-mean-squared error (RMSE) as a measure of the reconstruction error. The RMSE is defined as

$$\mathrm{RMSE} = \sqrt{\frac{\sum_i \sum_j |f(i,j) - g(i,j)|^2}{N}},$$

where f and g mean the ideal phantom and the reconstruction, respectively. And N is the total pixels of the image. The RMSEs of the reconstructions of the Shepp–Logan phantom are calculated and showed in Fig. 5 for two different methods. We can see that the ADTVM algorithm is obviously more accurate and effective.

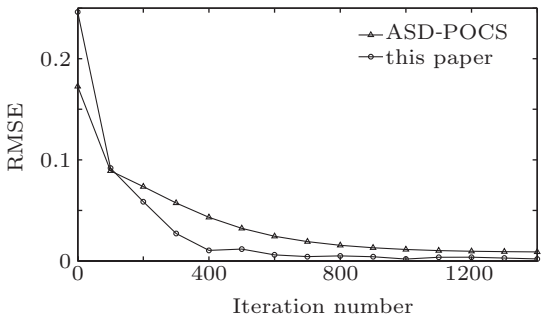

Fig. 5. Root-mean-squared errors each as a function of iterations for different methods in a 90°-LCT scan.

In the second set of configuration, the detector is split into two segments, which are arranged in a vertical distribution (shown in Fig. 6). A scanning object is moved linearly and the angle coverage is 45° in each segment. For this scan, the sampling points of the object in the Fourier space are described in Fig. 7. We can see that there exists a lack of four 45° ranges in the frequency domain.

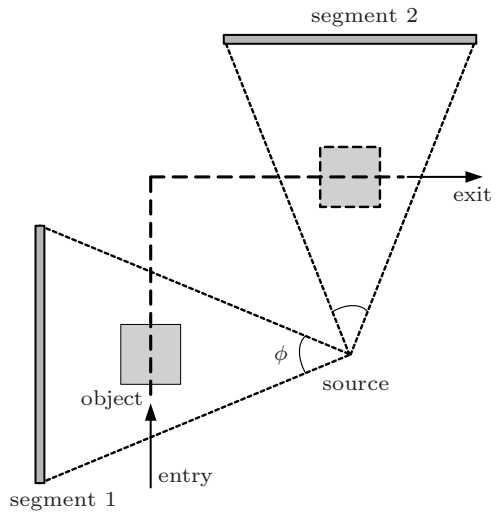

Fig. 6. Trajectories of two segments.

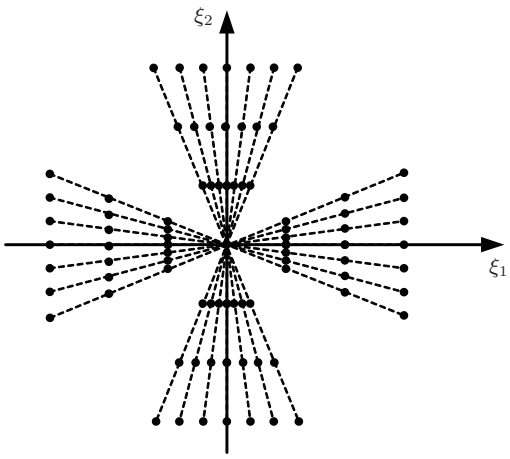

Fig. 7. Sampling points of a two-segment scan in the Fourier space.

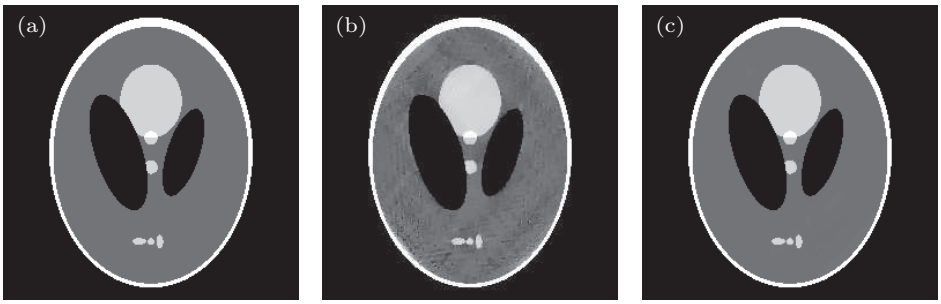

Fig. 8. Image reconstructions of the Shepp–Logan phantom in a two-segment LCT scan. Display window [0.1, 0.35]. Panel (a) shows the original image, panel (b) the result of ASD-POCS algorithm, and (c) the result of ADTVM algorithm.

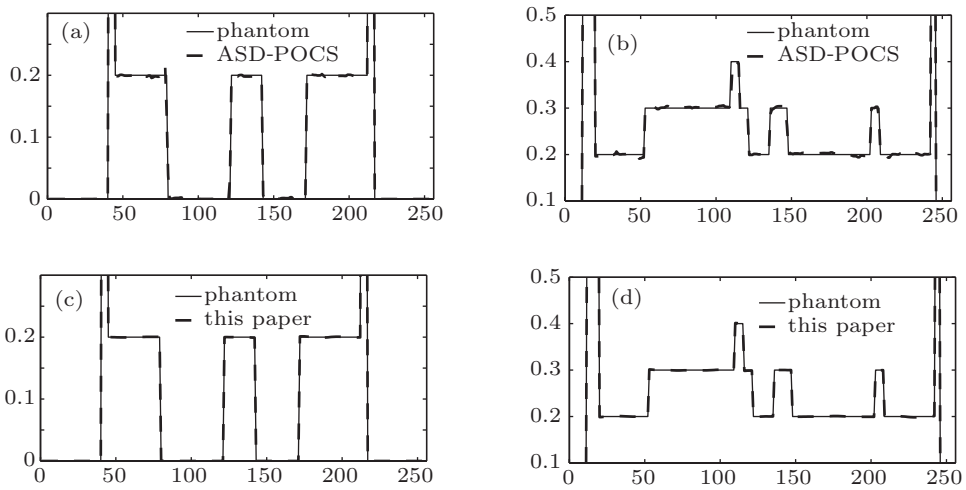

Fig. 9. Image profiles in Fig. 8, showing (a) horizontal profiles along the center of the ASD-POCS result, (b) vertical profiles along the center of the ASD-POCS result, (c) horizontal profiles along the center of the ADTVM result, and (d) vertical profiles along the center of the ADTVM result.

The reconstructed image results for both the ADTVM and ASD-POCS algorithms are shown in Fig. 8. The profiles of these images along the central horizontal and vertical rows are displayed in Fig. 9. The number of iterations for each reconstruction is 1000. As one can see, the ADTVM reconstruction is very close to the true phantom. On the other hand, the images obtained by use of the ASD-POCS algorithm are also reasonably accurate with only small distortions. We also study the root-mean-squared error as a function of iteration number. The result is displayed in Fig. 10. In a way the same as that in the first study, the accuracy of ADTVM method is better than the ASD-POCS method for the second scan.

Table 2 shows the RMSE of the reconstructions from the above projection data with different TV minimization algorithms. The run-time for our current implementation of the ADTVM algorithm is 0.14 s per loop for the phantom results in configuration 1.

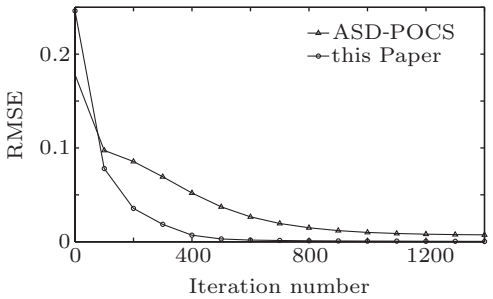

Fig. 10. Root-mean-squared errors each as a function of iterations for different methods in a two-segment LCT scan.

Table 2. The RMSE for the different methods.

	ASD-POCS		ADTVM	
Configuration	1 segment	2 segments	1 segment	2 segments
Iteration numbers	1000	1000	1000	1000
RMSE	1.138×10^{-2}	9.912×10^{-3}	1.925×10^{-3}	6.496×10^{-4}

3.2. Reconstruction using real data

To further check the capability of the proposed algorithm, we carry out the experiments to reconstruct a spark plug from real data. The real data are acquired with the CT system which is composed mainly of the X-ray source (YXLON FXE-225, Germany) and the flat-panel detector (Varian 4030E, USA) with a pixel size 0.127 mm. Because the effective angle coverage of source is nearly 30°, the scanning is split into four parts. The scanning trajectory is schematically illustrated in Fig. 11. The spark plug is moved linearly in each part, and rotates 30° between every two parts. Therefore, the total angle range is 120° experimentally. In each part of the scanning, the perpendicular distances from the source to the object center and to the detector are 86.88 mm and 484.47 mm, respectively. The sampling interval in the object trajectory is 0.6 mm and the total number of projections is $96 \times 4 = 384$.

We compare the proposed algorithm with LFBP,[7] SART, and ASD-POCS algorithms, the numbers of iterations for SART, ASD-POCS, and ADTVM reconstructions are all 200. The size of the reconstructed region is 200×200×170 with a voxel size of 0.15 mm×0.15 mm×0.15 mm. Figures 12 and 13 show the 110-th and 160-th z-axial reconstructed slice by the four methods, respectively, and figure 14 displays the 100-th x-axial reconstructed slice by the ASD-POCS and ADTVM methods.

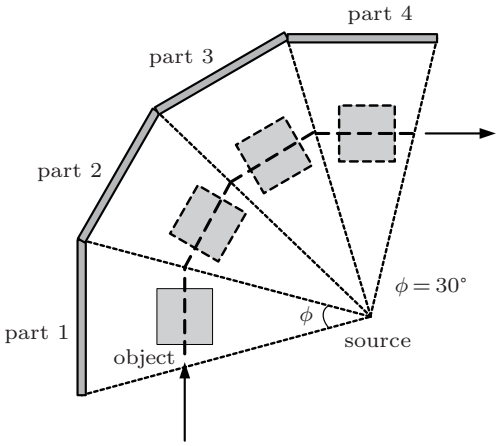

Fig. 11. Scan configuration of four parts.

From the reconstruction results using real data, it is found that the distortions and streaking artifacts are clearly seen in both LFBP reconstruction and SART reconstruction. Compared with these two methods, the ASD-POCS method and the proposed ADTVM method can effectively restrain the artifacts and improve the image quality, though the reconstruction images still have some artifacts on the edge of the missing data regions. Furthermore, it is interesting to note that the image artifacts are significantly less severe in the image reconstruction of ADTVM. The ADTVM appears to have less artifacts than the ASD-POCS reconstructions.

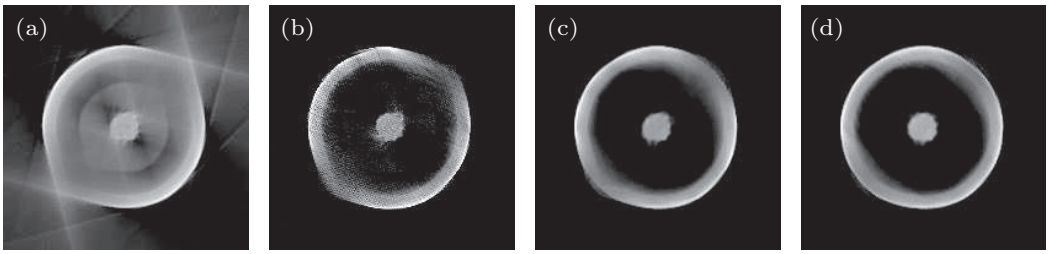

Fig. 12. The 110-th z-axial slices in three-dimensional (3D) image reconstruction of the spark plug. Panel (a) shows the result of LFBP, panel (b) the result of SART, panel (c) the result of ASD-POCS, and panel (c) the result of ADTVM.

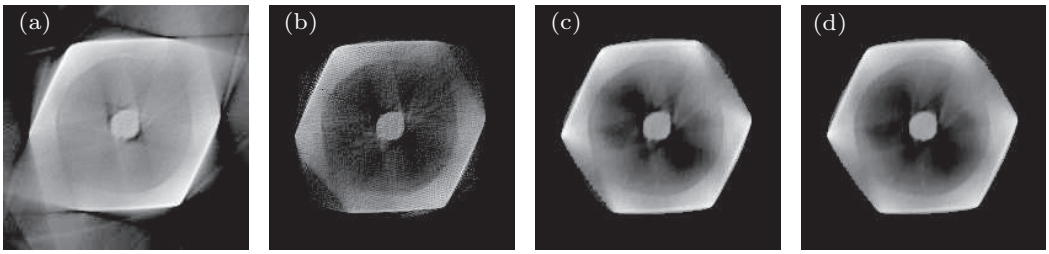

Fig. 13. The 160-th z-axial slices in 3D image reconstruction of the spark plug. Panel shows (a) the result of LFBP, panel (b) the result of SART, panel (c) the result of ASD-POCS, and panel (c) the result of ADTVM.

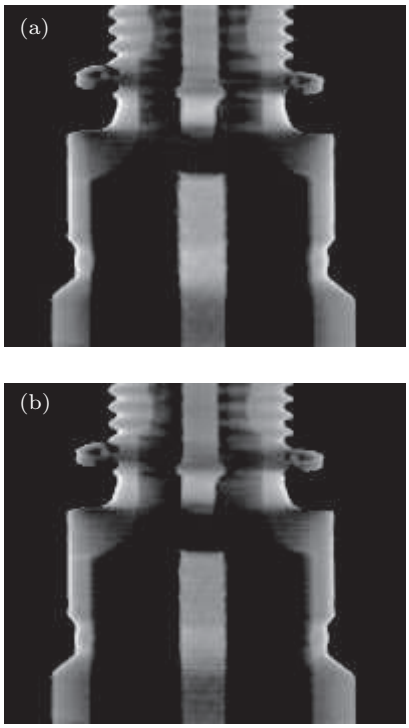

Fig. 14. The 100-th x-axial slices in 3D image reconstructions of the spark plug. Panel (a) shows the result of ASD-POCS, and panel (b) the result of ADTVM.

4. Discussion and conclusion

LCT is useful in the fields of online industrial scanning and security inspection due to its features of straight-line source trajectory and high scanning speed. However, because of the limitation of the ray-beam flare angle, the projection data sets are not sufficient for exact reconstruction. To cope with the limited-angle problem, we develop in this work an alternating direction TV minimization algorithm for LCT reconstruction based on augmented Lagrangian function. We evaluate and demonstrate the performance of the proposed algorithm in addressing both numerical simulation and real data reconstruction. To validate how the ADTVM algorithm can be applied to the LCT scanning and limited-angle problem, we make a comparison with the ASD-POCS algorithm. The experimental results show that both algorithms are able to effectively reconstruct quantitatively accurate images from imperfectly sampled data, in particular, ADTVM shows much faster convergence when applied to limited-angle data. The advantage of our new method is that the TV model is decomposed to two simple subproblems with closed form solution. Therefore, the ADTVM is efficient and practical for the low cost in each iteration.

Although this article presents the algorithm only in the context of linear scan CT, it is clear that the algorithm here is directly applicable to other tomographic imaging modalities.

References

[1] Pack J D, Noo F and Kudo H 2004 *Phys. Med. Biol.* **49** 2317
[2] Seger M M and Danielsson P E 2003 *Comput. Electron. Agric.* **41** 45
[3] Liu B D and Zeng L 2009 *J. X-ray Sci. Technol.* **17** 221
[4] Bleuet P, Guillemaud R, Desbat L and Magnin I 2002 *IEEE Trans. Nucl. Sci.* **49** 2366
[5] Gao H W, Zhang L, Xing Y X, Chen Z Q, Zhang J and Cheng J P 2007 *Opt. Eng.* **46** 077004
[6] Smith B D 1993 *IEEE Trans. Med. Imag.* **12** 10
[7] Gao H W, Zhang L, Chen Z Q, Xing Y X, Cheng J P and Qi Z H 2007 *Opt. Eng.* **46** 057003
[8] Sidky E Y, Zou Y and Pan X 2005 *IEEE Nuclear Science Symposium Conference Record*, October 23–29, 2005, Puerto Rico, USA, p. 2441
[9] Gao H W, Zhang L, Xing Y X, Chen Z Q and Cheng J P 2008 *IEEE Trans. Nucl. Sci.* **55** 552
[10] Tuy H 1983 *SIAM. J. Appl. Math.* **43** 546
[11] Gao H W, Zhang L, Xing Y X, Chen Z Q and Cheng J P 2006 *IEEE Nuclear Science Symposium Conference Record*, October 29–November 1, 2006, San Diego, California, USA, p. 2304
[12] Candes E, Romberg J and Tao T 2006 *IEEE Trans. Inf. Theory* **52** 489
[13] Candes E, Romberg J and Tao T 2006 *Commun. Pure Appl. Math.* **59** 1207
[14] Sidky E Y and Pan X 2008 *Phys. Med. Biol.* **53** 4777
[15] Gao H W, Xing Y X, Zhang L, Chen Z Q and Cheng J P 2007 *9th International Meeting on Fully Three-Dimensional Image Reconstruction in Radiology and Nuclear Medicine*, July 9–13, 2007, Lindau, Germany, p. 128
[16] Chen G H, Tang J and Leng S 2008 *Med. Phys.* **35** 660
[17] Sidky E Y, Kao C M and Pan X 2006 *J. X-ray Sci. Technol.* **14** 119
[18] Sidky E Y, Pan X, Reiser I S and Nishikawa R M 2009 *Med. Phys.* **36** 4920
[19] Lu X Q, Sun Y and Yuan Y 2011 *Pattern Recognition* **44** 2427
[20] Ritschl L, Bergner F, Fleischmann C and Kachelrieß M 2011 *Phys. Med. Biol.* **56** 1545
[21] Cho S, Lee T, Min J and Chung H 2012 *Opt. Eng.* **51** 080501
[22] Wang L Y, Li L, Yan B, Jiang C S, Wang H Y and Bao S L 2010 *Chin. Phys. B* **19** 088106
[23] Li C B 2009 *An Efficient Algorithm for Total Variation Regularization with Applications to the Single Pixel Camera and Compressive Sensing,* MS dissertation, Houston: Rice University, USA
[24] Wang Y L, Yang J F, Yin W T and Zhang Y 2008 *SIAM J. Imag. Sci.* **1** 248
[25] Li S P, Wang L Y, Yan B, Li L and Liu Y J 2012 *Chin. Phys. B* **21** 108703